Wavelet-based adaptive simulation of nonuniform interconnects with arbitrary loads

Wavelet-Based Adaptive Simulation of Nonuniform Interconnects oith Arbitrary Loads

S. Grivet-Talocia
Dip. Elettronica, Politecnico di Torino
Corso Duca degli Abruzzi 24
I-10129, Torino, Italy

F. Canavero
Dip. Elettronica, Politecnico di Torino
Corso Duca degli Abruzzi 24
I-10129, Torino, Italy

Abstract: This paper presents a wavelet-based adaptive discretization of the Nonuniform Multiconductor Transmission Lines. The resulting numerical scheme allows time-domain transient simulations of practical interest structures loaded with arbitrary dynamic and nonlinear termination networks. The advantage of the wavelet discretization is the usage of very few automatically determined unknowns for the computation of the solution at each time step. The adaptivity of the discretization does not affect the overall accuracy, which is the same as if a uniformly fine grid were used. The proposed scheme offers an optimized alternative to the more standard finite-difference (FDTD) approach for signal integrity analysis of interconnects.

INTRODUCTION

This paper presents a new time-domain simulation method for multiconductor interconnects loaded by arbitrary nonlinear and dynamic terminations. The proposed method allows to treat both uniform and nonuniform interconnects. The possibility to account for nonuniformities due to a non translation-invariant cross section allows to deal with complex structures like cables laid in automobiles or airplanes, or even nonparallel lands on PCB's. The signal integrity analysis of such structures is essential for a careful design under EMC constraints.

It will be assumed in the following that the interconnects may be analyzed under the assumption of the quasi-TEM mode of propagation, i.e., the longitudinal variations in the cross section are not too large, and the cross section itself is small with respect to the wavelength corresponding to the highest frequency in the system. Therefore, we will use the Nonuniform Multiconductor Transmission Lines (NMTL) equations as a starting point. Some considerations on the validity of these assumptions can be found in a companion paper in this record [1].

Several approaches have been presented for the simulation of interconnects. Among the schemes allowing the inclusion of arbitrary dynamic and nonlinear terminations, therefore performing simulation in the time-domain, the most widely used is the finite-difference (FDTD) method [3]. This popularity is due to its simplicity, flexibility, and robustness.

A standard FDTD scheme requires the spatial discretization of the line into a very fine grid when fast transients are to be modeled. However, looking at the voltages and currents at a fixed time along the line in a typical simulation, one can note that there are only few regions of fast spatial variations, while other parts of the solution are smooth. Therefore, a small separation between spatial nodes may be unnecessary for some regions along the line, although it is mandatory around the location of the singularities. The aim of this paper is to show that wavelet-based discretizations may be used to construct adaptive numerical schemes to perform simulation of nonuniform multiconductor transmission lines with arbitrary terminations. The results will show that the solution can be computed by using fewer unknowns than the standard FDTD nodal values.

PROBLEM STATEMENT

Under the quasi-TEM assumption any interconnect may be described through the NMTL equations [2]

$$\frac{\partial}{\partial z}\mathbf{v}(z,t) + \mathbf{L}(z)\frac{\partial}{\partial t}\mathbf{i}(z,t) + \mathbf{R}(z)\mathbf{i}(z,t) = 0, \quad (1)$$

$$\frac{\partial}{\partial z}\mathbf{i}(z,t) + \mathbf{C}(z)\frac{\partial}{\partial t}\mathbf{v}(z,t) + \mathbf{G}(z)\mathbf{v}(z,t) = 0. \quad (2)$$

The line is assumed to have $P+1$ conductors including the reference, and the per-unit-length parameters $\mathbf{L}(z)$, $\mathbf{C}(z)$, $\mathbf{R}(z)$, and $\mathbf{G}(z)$ are $P \times P$ matrices whose entries are arbitrary functions of the longitudinal coordinate z.

The line terminations will be modeled as arbitrary nonlinear and dynamic voltage-controlled multiports, described by their state equations. This model is derived from [3] where the solution of the resulting equations is obtained through the FDTD method. More precisely, the termination at $z = 0$ will be characterized by

$$\frac{d}{dt}\mathbf{x}_0(t) = \mathbf{f}_0(\mathbf{x}_0(t), \mathbf{v}(0,t), \mathbf{u}_0(t); t)$$

0-7803-5057-X/99/$10.00 © 1999 IEEE

$$\mathbf{i}(0,t) = \mathbf{g}_0(\mathbf{x}_0(t), \mathbf{v}(0,t), \mathbf{u}_0(t), \frac{d}{dt}\mathbf{u}_0(t); t) \quad (3)$$
$$+\mathbf{Q}_0 \frac{d}{dt}\mathbf{v}(0,t),$$

where $\mathbf{x}_0$ is a state-variable vector, $\mathbf{u}_0$ is a vector including the independent sources, and $\mathbf{f}_0$, $\mathbf{g}_0$ are nonlinear functions. The matrix $\mathbf{Q}_0$ allows to include the effect of lumped shunt capacitors. A similar model is considered for the termination network at $z = \mathcal{L}$, for which the suffix $_1$ is used. The solution of the mathematical problem expressed by Eqs. (1)-(2) and (3) does exist in all cases of practical interest. However, some theoretical considerations on the existence and uniqueness of the solution can be found in [4].

DISCRETIZATION

The discretization of the NMTL equations is obtained through application of the TDSE (Time-Domain Space Expansion) method introduced in [5]. The method is based on a weak formulation of the NMTL equations obtained by expanding voltages and currents into a given set of basis functions, and by testing the resulting equations through another set of possibly different basis functions. The functions employed in [5] were piecewise polynomials (B-splines). We will adopt here biorthogonal wavelet functions [6, 7] derived from B-spline systems. In this section we briefly recall the spatial discretization scheme without specific reference to the choice of basis functions. The next section will focus on the wavelet bases that will be actually used for the computations.

Let us denote $\{\eta_n(z), n = 1, .., N\}$ as the set of trial functions. The representation of voltages and currents will be

$$\mathbf{v}(z,t) = \sum_{n=1}^{N} \mathbf{v}_n(t)\eta_n(z), \quad \mathbf{i}(z,t) = \sum_{n=1}^{N} \mathbf{i}_n(t)\eta_n(z). \quad (4)$$

Testing the NMTL equations by taking products with each function in the set $\{\xi_n(z), n = 1, .., N\}$ and then integrating, we get a discretized system of ODE's, where the expansion coefficients $\mathbf{v}_n(t)$ and $\mathbf{i}_n(t)$ are the unknowns. The equations of the terminations can be combined with this system by eliminating the border current coefficients $\mathbf{i}_1$ and $\mathbf{i}_N$ in terms of the voltage coefficients $\mathbf{v}_1$ and $\mathbf{v}_N$ and of the state variables $\mathbf{x}_0$, $\mathbf{x}_1$. This procedure involves a straightforward substitution and is not further detailed here. The result is a global system of ordinary differential equations which reads

$$\mathbf{\Psi} \frac{d}{dt}\mathbf{y}(t) = \mathbf{\Phi}\, \mathbf{y}(t) + \mathcal{F}(\mathbf{y}(t)), \quad (5)$$

where the vector $\mathbf{y}$ includes the expansion coefficients of voltages and currents as well as the state-variable vectors of the terminations, the matrices $\mathbf{\Psi}$ and $\mathbf{\Phi}$ are highly sparse, and the nonlinear function $\mathcal{F}$ involves only the few border coefficients and the state variables of the termination networks.

It was shown in [5] that when the trial and test functions constitute biorthogonal sets, the matrix $\mathbf{\Psi}$ reduces to the identity. This is not true if more traditional functions, like e.g. triangle functions or higher order finite element functions, are used in a Galerkin scheme. The wavelet bases that we will use are indeed pairs of biorthogonal systems, and will lead to a fully explicit system of ODE's (i.e., $\mathbf{\Psi} = \mathcal{I}$). The system (5), in either implicit or explicit form, can be solved by a suitable time stepping algorithm. Possible choices will be discussed in the forthcoming sections.

WAVELET BASES

This section is devoted to the description of the wavelet bases that will be used for the discretization of the NMTL equations. After a brief introduction to hierarchical approximation spaces, which form the abstract framework in which wavelet approximations are embedded, we will describe the particular set of wavelets that are employed in this work to perform the numerical simulations. This section is not intended as a tutorial on wavelets, but only as a quick summary of the main properties of wavelets that are of some relevance for this work. For further details we recommend the many books and papers already available on the subject (see, e.g., [8, 9]).

Hierarchical Approximation Spaces

Consider a function $v \in L^2$ defined on a domain $\Omega \subseteq \mathbf{R}$. We want to approximate v by performing its projection onto a suitable approximation space V_j,

$$v_j = P_j v, \qquad P_j : L^2 \to V_j. \quad (6)$$

The index j, henceforth denoted as *refinement level*, controls the accuracy of the approximation, i.e., the space V_j converges to the full space L^2 when $j \to \infty$. In addition, we require that the approximation spaces are nested for increasing refinement levels. In other words, we can construct the sequence

$$V_{j_0} \subseteq \cdots \subseteq V_j \subseteq V_{j+1} \subseteq \cdots \subseteq V_J \subseteq L^2. \quad (7)$$

The levels j_0 and J, which can be defined a priori, define the coarsest and finest approximations, respectively.

The basic idea behind wavelets is to express the approximation at level $j+1$ through a *hierarchical* representation, obtained by decomposing the space V_{j+1} into a coarser approximation space V_j plus some detail space W_j,

$$V_{j+1} = V_j \oplus W_j. \quad (8)$$

Iterating through the entire range of refinement levels we get the unique decomposition

$$V_J = V_{j_0} \oplus \bigoplus_{j=j_0}^{J-1} W_j. \quad (9)$$

The basis functions ψ_{jk} of these detail spaces W_j are zero-mean functions, and are called *wavelets*, while the basis functions φ_{jk} of the approximation spaces V_j are called *scaling functions*. Note that these functions are labelled by two indices, the first representing the refinement level, and the second distinguishing different functions at the same level. According to Eq. (9), we can give two alternative representations in terms of basis functions of the approximation v_J, respectively,

$$v_J = \sum_k c_{J,k}\varphi_{J,k}, \tag{10}$$

$$v_J = \sum_k c_{j_0,k}\varphi_{j_0,k} + \sum_{j=j_0}^{J-1}\sum_k w_{jk}\psi_{jk}. \tag{11}$$

The first representation is called *canonical*, because it is the usual form in which finite element approximations are expressed. For example, one could replace the functions $\varphi_{J,k}$ with triangle functions (or, equivalently, linear finite elements), and the coefficients $c_{J,k}$ would be the nodal values of the original function v. The second representation is called *hierarchical*, because it involves the iterative superposition of details at increasing levels j without modifications of the coarser parts of the approximation. It should be noted that a change of basis between the canonical and hierarchical representation (and viceversa) can be performed through fast algorithms involving only $O(N)$ operations, i.e., faster than FFT, which requires $O(N \log N)$ operations.

The scaling functions and wavelets with any indices (j,k) are obtained through dilations and translations of single generating functions φ and ψ,

$$\begin{aligned}\varphi_{jk}(x) &= 2^{j/2}\varphi(2^j x - k),\\ \psi_{jk}(x) &= 2^{j/2}\psi(2^j x - k).\end{aligned} \tag{12}$$

It should be noted from these expressions that the detail functions ψ_{jk} are characterized by a highpass-like spectrum, which is concentrated towards higher and higher frequencies as the level j increases. Therefore, the hierarchical decomposition (11) can be regarded as the decomposition of v_J into a set of frequency bands. As we add more details at higher j, we extend the range of frequencies included in the approximation, and we get convergence in L^2 sense.

The main advantage in the hierarchical decomposition is that the wavelets ψ_{jk} can be designed to be extremely localized in space around the points $x_{jk} = (k + 0.5)\ 2^{-j}$. From Eq. (12), in fact, we see that the support decreases exponentially as j increases. Therefore, if the function v to be approximated is characterized by a small region with fast variations and is smooth elsewhere, it can be shown that only a small portion of the coefficients w_{jk} should be retained. The theory of wavelets shows that the location and the number of needed details can be automatically

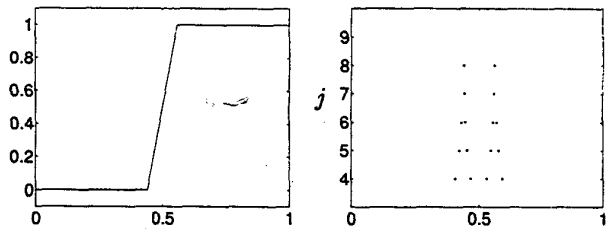

Figure 1: Left panel: adaptive approximation of a step function with finite rise time. Right panel: location of the wavelet coefficients larger than 10^{-4}.

determined by looking at the magnitude of the wavelet expansion coefficients. This leads to extremely sparse representations, which can be *adapted* to the function v being analyzed. In summary, we obtain the adapted representation

$$v \simeq \sum_k c_{j_0,k}\varphi_{j_0,k} + \sum_{j,k\in\Lambda_\epsilon} w_{jk}\psi_{jk}, \tag{13}$$

where

$$\Lambda_\epsilon = \{(j,k) : |w_{jk}| > \epsilon\} \tag{14}$$

and ϵ is a threshold controlling the accuracy/sparseness of the approximation.

The high degree of sparsity of wavelet-based adaptive representations is best illustrated with an example. Figure 1 shows a step function with a finite rise time, which is constructed as a piecewise linear function. The left panel is the actual approximation with a maximum level $J = 10$, corresponding to 1025 basis functions in the canonical representation and to only 35 in the adapted representation. The right panel illustrates the location x_{jk} of the wavelet coefficients w_{jk} larger than $\epsilon = 10^{-4}$ used to construct the approximation. For clarity, the coefficients have been differentiated through refinement levels. The sparsity of the overall representation and the adaptivity to the regions of fast variation are evident from the figure.

Biorthogonal B-Splines Wavelets

The scaling functions and wavelets can be orthogonal, with the decomposition of Eq. (9) obtained through orthogonal sums. This setting is widely used in the literature [11]. However, it can be shown that orthogonal wavelets cannot be at the same time symmetric and compactly supported [9]. Symmetry is convenient for the implementation of numerical schemes, while a compact support is essential when complicated boundary conditions are to be enforced. These two features can be recovered if orthogonality is released in favor of the more general biorthogonality [9]. This requires to introduce dual scaling functions $\widetilde{\varphi}_{jk}$ and wavelets $\widetilde{\psi}_{jk}$. These are characterized by the same properties as the primal functions φ_{jk} and ψ_{jk}, and are mainly

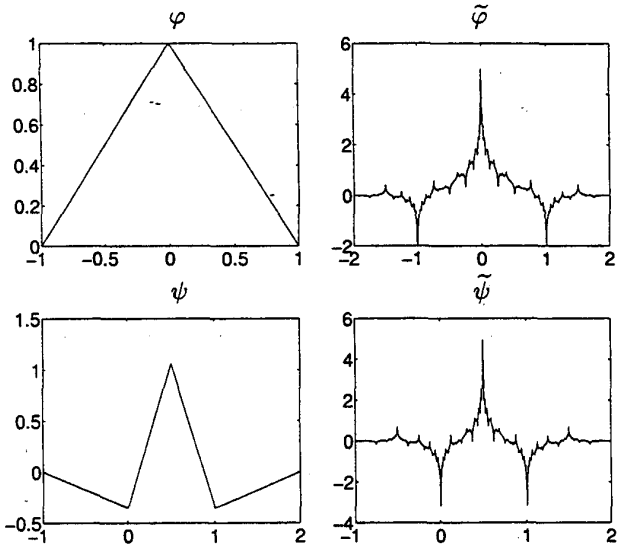

Figure 2: Biorthogonal B-splines scaling functions (top row) and wavelets (bottom row) with two vanishing moments.

used for the computation of the expansion coefficients in Eq. (11). More precisely, with reference to Eq. (11), we have the following identities

$$c_{jk} = \langle v, \widetilde{\varphi}_{jk} \rangle, \qquad w_{jk} = \langle v, \widetilde{\psi}_{jk} \rangle. \tag{15}$$

In this work we will use a special case of biorthogonal wavelets, namely the biorthogonal B-splines wavelets, which were originally introduced in [9]. The main feature of this system, beyond symmetry and compact support, is that the primal scaling functions are B-splines, i.e., piecewise polynomials of a fixed degree. Also the primal wavelets, which can be expressed as linear combinations of the scaling functions, are piecewise polynomials of the same degree. The construction of the dual scaling functions and wavelets is detailed in [9]. We report in Fig. 2 the particular functions that we will be using in the following. These are constructed from piecewise linear B-splines by enforcing two vanishing moments for the wavelets. It should be noted that the dual functions (right panels) are poorly regular. However, these functions will be only used as test functions in the TDSE framework. Therefore, no regularity is needed. We only need to be able to compute the testing integrals. This can be performed through simple and highly optimized algorithms that make use of special properties of wavelets. Further details can be found in [10].

When the domain is the whole real line, we can construct each scaling function and wavelet with indices (j,k) through dilations and translations according to Eq. (12). Similar expressions hold for the duals $\widetilde{\varphi}_{jk}$ and $\widetilde{\psi}_{jk}$, with corresponding dual generators. Instead, when the domain is bounded, such in the case of the unit interval $[0,1]$, special border functions have to be defined, while the dilation and translation process of Eq. (12) remains valid for those scaling functions and wavelets with support strictly included in the domain. We cannot include in this paper the details of the construction of the border functions. We refer the reader to [7] and references therein for a complete derivation.

ACCURACY AND TIME DISCRETIZATION

In this section we use a simple hyperbolic test equation to investigate the accuracy of the wavelet discretization. The main result will be the proof that the TDSE method with piecewise linear biorthogonal B-spline wavelets is fully equivalent to a fourth-order finite difference method. Consequently, the present method represents an improvement with respect to the standard FDTD scheme, which is only a second order scheme.

Let us consider the simplest hyperbolic equation,

$$u_t(z,t) + a u_z(z,t) = 0, \qquad z \in \mathbf{R}. \tag{16}$$

where the subscript indicates partial differentiation and a is a constant. We consider an unbounded domain because we are not interested in the boundary conditions at this stage. If we apply the TDSE discretization to Eq. (16) using $\varphi_{J,m}$ as trial functions and $\widetilde{\varphi}_{J,k}$ as test functions at a given refinement level J, we get a system of ODE's for the expansion coefficients c_m. If we use as trial and test functions the piecewise linear B-splines scaling functions of Fig. 2 (top row), we can compute analytically the projection integrals, obtaining

$$\frac{d}{dt}c_k + \frac{a}{12\Delta z}(c_{k-2} - 8c_{k-1} + 8c_{k+1} - c_{k+2}) = 0 \tag{17}$$

for any k, where $\Delta z = 2^{-J}$ is the spatial resolution of the approximation.

If we indicate now with v_k and v'_k the nodal values of the solution and its spatial derivative,

$$v_k(t) = u(k\Delta z, t), \qquad v'_k(t) = u_z(k\Delta z, t), \tag{18}$$

we can derive the expression of a fourth-order centered finite-difference approximation of the spatial derivative in eq. (16). We skip the derivation, which leads to the expression [12]

$$v'_k \simeq \frac{1}{12\Delta z}(v_{k-2} - 8v_{k-1} + 8v_{k+1} - v_{k+2}). \tag{19}$$

This expression matches exactly the one in Eq. (17). Recalling now the full equivalence between the canonical and the hierarchical representation in Eqs. (10)-(11), we are led to the conclusion that even if we use wavelet bases the resulting discretization scheme is fully equivalent to a fourth-order finite-difference approximation.

Given this equivalence, it is necessary to select a proper time integration method in order to preserve the high accuracy of the space discretization. If a standard leapfrog scheme is used [3], we only get second order accuracy in time. Moreover, it can be shown [12] that the stability limit for leapfrog in time with fourth-order differencing in space is $\Delta t \leq 0.72\Delta z/a$, i.e., the time step must be smaller than the Courant condition for standard FDTD. In addition, if a homogeneous term is added to the equation (like the terms in the NMTL equations representing losses), the resulting scheme is not stable for any choice of Δt. For this reason we are led to choose another possibly high-order time integration scheme that is capable of preserving stability. We found that the optimal choice is a fourth-order Runge-Kutta scheme [12]. In fact, the accuracy of this time discretization matches the accuracy of the spatial discretization, which is desirable for hyperbolic equations, and in addition the stability limit requires only the time step to satisfy $\Delta t \leq 2.06\Delta z/a$.

The solution of explicit system of ODE's through the fourth-order Runge-Kutta scheme requires to evaluate four times the time derivative of the unknowns, i.e., the right-hand side of Eq. (5), at each time step. The key advantage of the present method with respect to the standard FDTD scheme is the possibility of performing these evaluations in a very fast way. Indeed, many of the unknowns in the array y are zero due to the wavelet representation. More precisely, the cardinality of the set Λ_ϵ (see Eq. 14) is usually very small. In addition, due to the fact that the NMTL equations are hyperbolic and the speed of propagation is finite, it is possible to know a priori where the location of the regions of fast variations in the solution will be at the next time step. Consequently, the time-stepping involves at each iteration very few unknowns, while the others will remain equal to zero. More details on this adaptive time-stepping will be given in a forthcoming paper.

RESULTS

We proceed now with two examples. The first is a uniform scalar transmission line with normalized characteristic impedance and delay time ($Z_0 = 1, T = 1$) excited by a unitary step generator with rise time $\tau = 0.3T$ and unitary internal resistance, and loaded with a capacitor ($C = 1$) and a diode in parallel. We chose this simple validation example because it can be readily analyzed with SPICE. The top panel of Fig. 3 shows the voltages at the two line terminations, indicating excellent agreement between the wavelet and the SPICE simulations. The bottom panel of Fig. 3 shows the location in the $[z, t]$ plane of the significant wavelet coefficients actually used for the computations. It can be noted that very few coefficients are needed, and that these coefficients are located around the characteristic curves along which the fast variations of the solution occur.

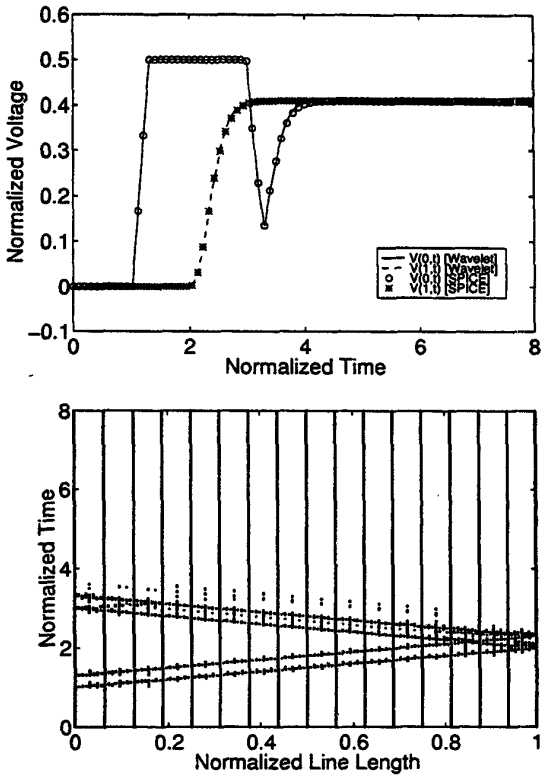

Figure 3: Top panel: normalized voltages at the terminations of a scalar transmission line excited by a step generator and loaded with a capacitor and a diode. Bottom panel: locations of the significant voltage wavelet coefficients actually used for the computation of the solution.

The second example is a more realistic structure, depicted in Fig. 4. It consists of two nonparallel PCB lands over a ground plane. The voltage pulse $v_s(t)$ is a 5 V step with rise time $\tau = 200$ ps. The cross-section of the interconnect is electrically small throughout the significant frequency spectrum of this waveform, therefore a quasi-TEM propagation of the fields can be assumed and Eqs. (1)-(2) are valid (see [1]). The crosstalk voltages at the left and right terminations are reported in the top panel of Fig. 5, while the locations of the significant voltage wavelet coefficients are reported in the bottom panel. Also in this case the solution was computed by using very few coefficients.

CONCLUSIONS

In conclusion, the presented adaptive approach is able to identify in a time-marching scheme the structure of the solution, to automatically detect which are the significant

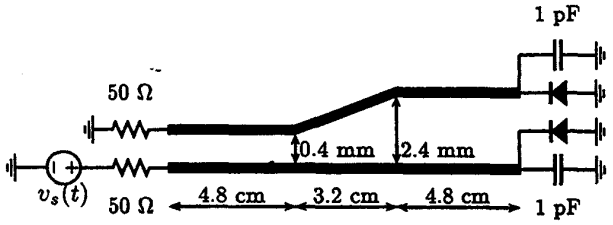

Figure 4: Typical PCB configuration (top view) with nonparallel traces and termination networks. The width of the traces is 0.2 mm. The structure is above a reference ground plane and a dielectric substrate 0.6 mm high with $\varepsilon_r = 4.7$.

wavelet expansion coefficients needed to represent the solution with a suitable accuracy, and to perform the computation by using only those significant coefficients. Therefore, this method seems to be very promising in further reducing the computational cost of existing non-adaptive methods.

REFERENCES

[1] F. Canavero and S. Grivet-Talocia, "Accuracy of propagation modeling of transmission lines", *Proc. IEEE Int. Symposium on EMC*, August 2–6, 1999, Seattle, WA.

[2] C. R. Paul, *Analysis of Multiconductor Transmission Lines*, John Wiley and Sons, NY, 1994.

[3] A. Orlandi and C. R. Paul, "FDTD Analysis of Lossy, Multiconductor Transmission Lines Terminated in Arbitrary Loads", *IEEE Trans. Electromagn. Compat.*, vol. 36, 1996, 388–398.

[4] A. Maffucci and G. Miano, "On the Dynamic Equations of Linear Multiconductor Transmission Lines with Terminal Nonlinear Multiport Resistors", *IEEE Trans. Circ. Systems I*, vol. 45, 1998, 812–829.

[5] S. Grivet-Talocia, F. Canavero, "Time Domain Space Expansion Solution of the Nonuniform Multiconductor Transmission Lines", *Proc. Int. Symposium on EMC*, September 14-18, 1998, Rome, Italy, 610–614.

[6] S. Grivet-Talocia and F. Canavero, "Wavelet-based adaptive solution for the nonuniform multiconductor transmission lines," *IEEE Microwave and Guided Wave Letters*, vol. 8, pp. 287–289, August 1998.

[7] S. Grivet-Talocia and A. Tabacco, "Wavelets on the interval with optimal localization", to appear in *Mathematical Methods and Models in Applied Sciences.*

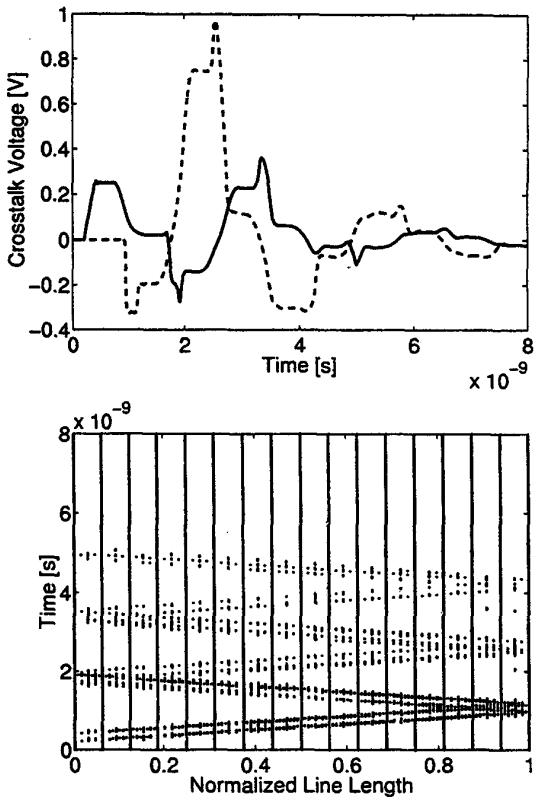

Figure 5: Top panel: crosstalk voltages at the left (continuous line) and right (dashed line) terminations of the interconnect of Fig. 4. Bottom panel: locations of the significant voltage wavelet coefficients actually used for the computations.

[8] I. Daubechies, *Ten Lectures on Wavelets*, CBMS-NSF Series in Applied Mathematics 61, SIAM, Philadelphia, 1992.

[9] A. Cohen, I. Daubechies, J. Feauveau, Biorthogonal bases of compactly supported wavelets, *Comm. Pure Appl. Math.*, **45**, 1992, 485-560.

[10] W. Dahmen, C. Micchelli, Using the refinement equation for evaluating integrals of wavelets, *SIAM J. Num. Anal.*, **30**, 1993, 507-537.

[11] L. Katehi, M. Krumpholz (Eds.), Special Issue on Wavelets in Electromagnetics, *Int. J. Num. Model.*, **11**, 1998, 1-96.

[12] B. Gustafsson, H.O. Kreiss, J. Oliger, *Time Dependent Problems and Difference Methods*, Wiley, New York, 1995.